JOURNAL OF AIRCRAFT
Vol. 41, No. 5, September–October 2004

Effects of Synthetic Jet Actuation on a Ramping NACA 0015 Airfoil

Lance W. Traub,* Adam Miller,† and Othon Rediniotis‡
Texas A&M University, College Station, Texas 77843-3141

An experimental investigation was undertaken to evaluate the effectiveness of a synthetic jet actuator (SJA) for flow control on a pitching airfoil. A NACA 0015 profiled airfoil was ramped up at various rates with concomitant surface-pressure acquisition. A self-contained synthetic jet actuator was positioned in the interior of the airfoil. Synthetic-jet-actuation parameters included the jet-momentum coefficient and the slot exit width. The behavior of the surface pressures is investigated as well as their integrated properties. The data suggest that the effect of the SJA is to delay the onset of the dynamic-stall vortex formation to higher incidence and in some cases, for the parameters and incidence range investigated, suppress it totally. However, in the instances when formed, the synthetic jet appears to increase the loading induced by the stall vortex. At low ramp rates, the synthetic jet forcing causes the formation of a stall vortex where the unforced data showed a psuedostatic stall-type behavior. Hot-wire anemometer surveys of the jet exit showed that compressibility effects would manifest for small slot exit areas and increase with frequency. Variation of the SJA driving frequency showed the ability to control the flow from massively separated to fully attached at 25-deg instantaneous angle of attack.

Nomenclature

Cl	=	sectional lift coefficient, $l/0.5\rho U^2 c$
Cm	=	sectional quarter-chord pitching-moment coefficient, $m/0.5\rho U^2 c^2$
$C\mu$	=	jet-momentum coefficient, $2V_{\text{rms}}^2 sw/U^2 c$
c	=	airfoil chord, 420 mm
F^+	=	nondimensional actuator frequency, fx/U
f	=	actuator frequency, Hz
K	=	incompressible parameter
k	=	nondimensional ramp rate, $\omega c/U$
l	=	sectional lift, N
m	=	sectional pitching moment, Nm
sw	=	slot width, mm
T	=	period, $1/f$
t	=	time, s
U	=	freestream velocity, m/s
u	=	local velocity, m/s
V	=	jet velocity, m/s
x	=	length from the actuator slot to the airfoil trailing edge, mm
Z_{normal}	=	local coordinate perpendicular to airfoil surface
ω	=	angular ramp rate, rad/s

Subscripts

max	=	maximum
rms	=	root mean square

Introduction

THE evolution of aerodynamics has been heavily influenced by the pursuit of maximum efficiency. Until recently, these advances were rooted in the configuration design routines employed. However, significant advances in flow control and its application have provided another means whereby aerodynamic efficiency and functionality can be improved. The ongoing research effort has also spawned the desire to achieve hingeless control for aircraft, unmanned aerial vehicles, submersibles, etc. These efforts are motivated by potential weight savings, increased actuator robustness, and stealth benefits. In addition, flow control has the potential to attenuate undesirable aerodynamic phenomena that can affect control or impair aerodynamic performance. Although not new as a concept, flow control has taken great strides with the application of novel devices to help maintain the desired flow patterns around a body. Traditionally, wing efficiency would be achieved through attention to design; however, off-design performance could not be guaranteed. Flow control, either passive or active, seeks to modify the flow such that it behaves in a different manner compared to no control and essentially increases the off-design envelope or the ability of the wing to function at extreme attitudes. The flow control can be used to control or promote boundary layer transition, limit flow separation, augment lift, modify acoustic emissions, or reduce drag. In addition, rapidly pitching aircraft can suffer from the formation of a so-called dynamic stall vortex (D.S.V.), which can have a deleterious effect on aircraft stability. It would be of value to determine the ability of flow control to attenuate or modify the D.S.V. formation so as to potentially augment aerodynamic performance.

Methods for passive flow control include vortex generators,[1] distributed roughness, acoustic cavities,[2] or self-excited rods.[3] All of these methodologies try to limit separation either by augmenting boundary layer momentum through enhanced mixing or introducing transverse velocity fluctuations in the vicinity of the airfoil[3] (self-excited rod). Active methods for flow control include blowing,[4] suction,[5] moving surface elements,[6] oscillatory blowing/suction,[7] wall oscillation,[8] vibrating ribbons,[9] and zero-mass-flux, finite momentum actuators or synthetic jet actuators (SJAs).[10–13] The aforementioned techniques either remove low-energy boundary layer fluid (suction) or essentially increase boundary layer momentum (flow-injection methods) with additional mixing due to generation of coherent vortical structures (SJAs). Flow control can also be achieved using dynamic wing motion as shown in Refs. 14 and 15.

The mechanism for synthetic jet operation is well documented.[16] Shear layers are, in general, highly receptive to disturbances. The SJA serves as a forcing function, which when pulsed in the correct frequency range can cause the shear layer to resonate, which is associated with the formation of coherent structures. The shear layer generally locks into the driving frequency, or one of its harmonics. As a result, the shear layer forms discrete vortices, which then pair or merge, ultimately forming larger, stronger coherent structures

Received 1 July 2003; revision received 3 November 2003; accepted for publication 3 November 2003.

*TEES Research Scientist/Lecturer, Aerospace Engineering Department.
†Graduate Student, Aerospace Engineering Department. Student Member AIAA.
‡Associate Professor, Aerospace Engineering Department. Member AIAA.

with reduced frequency. As they advect downstream, these vortices behave in a similar fashion to those injected by conventional vortex generators. They mix high-momentum freestream fluid into the boundary layer, energizing it. Increasing the forcing frequency causes the formation of smaller, more closely spaced discrete vortices. Excessive forcing frequency can impair the merging of the resulting small shear-layer vortices such that the formation of effective mixing structures is weakened.[16]

Of the active methods, the SJA has received considerable attention as a compact, efficient actuator that can achieve effective flow control with considerably less complexity and energy expense then other active techniques. All SJA actuators basically consist of a cavity, which is bounded by a moving wall on one side, and an inlet/exit slot on another. Oscillation of the wall (or piston—depending on the particular method of implementing the jet) causes a periodic inflow and outflow of fluid, such that no net mass is transferred. A momentum balance over the exit slot indicates that momentum transfer is finite, as the inflow area greatly exceeds that of outflow. The jet can be exhausted in a Coanda fashion, parallel to the surface, or can be inclined relative to the surface for so-called virtual shaping, such that the potential pressure distribution around the wing is altered. The ability of SJAs to suppress flow separation is well documented.[10,11] The compact nature of the SJA design can also allow the device to be placed locally where required without the need for pneumatic ducting, if the SJA is designed to be electrically powered. The existing literature presents promising applications of the synthetic jet technology to flow separation under both laboratory and flight conditions.[17–20] Research includes investigation of the use of synthetic jet actuation for modifying the lift, drag, and flight-control characteristics of unconventional airfoils as well as flow separation over bluff bodies.[21–23] This technology could lead to elimination, reduction, or manipulation of steady and unsteady flow separation over a wing/blade, via active flow control and in a hingeless manner (no conventional moving control surfaces).

In most efforts in the existing literature, the SJAs are either powered piezoelectrically[21,22] or are powered from external hardware,[17,19,20] for example, pneumatic or acoustic mechanisms, with most of the hardware residing outside the test section. However, for most air and water vehicle applications the SJAs will need to be compact in order to be housed inside the control surface of the body whose aerodynamic/hydrodynamic characteristics they are trying to modify. Piezoceramic-based synthetic jet actuators, which can be small enough to be housed inside the control surface, can exhibit performance deterioration when operating at frequencies away from the actuator resonance frequencies and have limited maximum amplitudes. To address the need for compact, high-power synthetic jet actuators, we have developed a new, piston-based SJA. The actuator and its characterization are described here only in relation to the specific wind-tunnel experiments presented in this work; more detailed descriptions of the actuator can be found in Refs. 10 and 11.

A characteristic of a stalled airfoil is a pronounced negative pitching moment, induced by the lack of pressure recovery over the aft airfoil section. As SJAs can control the extent of flow separation, the significant pitching moment induced by the movement of the airfoil's center of pressure, as the flow separates, presents itself as a natural mechanism to generate moments for hingeless pitch control at high angles of attack. Existing static pitch data[10] indicate that this methodology would be effective; however, effectiveness for a dynamically pitched wing has not been ascertained. When a wing is ramped beyond the static-stall angle, the motion maintains the inviscid nature of the flow delaying the forward progression of the trailing-edge stall (for moderate to thick airfoils), with boundary layer development aided through the leading-edge jet effect.[24] At higher incidence, viscous effects manifest causing stall. However, if the ramp rate is sufficiently high, and depending on aerofoil and freestream parameters, a collision of reversed flow near the leading-edge (caused by the significant adverse pressure gradient aft of the leading-edge suction peak) with the oncoming airstream can cause boundary layer liftoff with formation of a so-called dynamic-stall vortex. The vortex, in turn, causes a secondary boundary layer eruption. Interaction of this ejected vorticity and the D.S.V. feeding sheet causes detachment; this is a similar interaction mechanism to that of the secondary vortices and primary vortex feeding sheet over a delta wing with freestream disturbances.[25] As this vortex advects rearward over the surface, it causes significant pitching-moment fluctuations. The stall vortex forms closer towards the wing leading edge on a two-dimensional wing than a three-dimensional wing.[26] Greenblatt and Wygnanski[17] have shown that a SJA can reduce dynamic effects and moment excursions on a pitch-oscillating wing.

In this paper, an experimental investigation into the effects of the actuator on the pressures, forces, and moments recorded over a pitching airfoil are explored. The study is aimed at expanding the database of SJA applications in dynamic motions and specifically to ramp and hold motions. The ability of a SJA to generate pitching moments suitable for control at high incidence during ramp-type motions is also evaluated. Presented data includes surface pressures, SJA exit slot velocity measurements, upper-surface instantaneous boundary layer profiles, and integrated loads and moments.

Experimental Equipment and Procedure

The SJA driving mechanism consists of a dc motor with its shaft connected eccentrically to a crank, which is in turn connected to the piston of the SJA. Because of the eccentricity, the rotary motion of the motor is translated to linear motion of the SJA membrane/piston. This design offers benefits over piezoceramic driving mechanisms because it can achieve membrane/piston oscillation amplitudes at least an order of magnitude higher; it eliminates the dependence of oscillation amplitude on the oscillation frequency, which can be problematic for piezoceramic mechanisms; with available state-of-the-art, high power-density electric motors, it can match and exceed the power densities of piezoceramic mechanisms; it requires significantly smaller driving voltages. At present the actuator can operate at frequencies up to about 120 Hz. Consequently, for practical freestream velocities the actuator is limited to nondimensional frequencies F^+ of $\approx$1.5. This value is significantly lower then that achieved using piezoelectric actuators.[12] However, studies have indicated that the optimal F^+ range is approximately 0.5 to 1.5 (Refs. 19 and 22), representing two to four advecting vortical structures over the upper wing surface at any time instance. Consequently, the limitation on F^+ for the present actuator design is not viewed as a significant hindrance in the spirit of the present study.

For the present SJA, as shown in Fig. 1, electric motors drive a series of off-the-shelf small gasoline engines, which are used as reciprocating compressors. The cylinder head of each of these engines is open and attached to a plenum, which is closed on all sides except for a slot machined on one of the walls. The change in the cavity volume of the plenum causes the pressure inside the cavity to fluctuate, creating the synthetic jet. The use of the available engine technology reduces the effort to manufacture pistons with no leakage, thus simplifying the design and construction of the SJA. As shown in Fig. 1, the present SJA array is composed of six reciprocating compressors (pistons), which are driven by two dc motors.

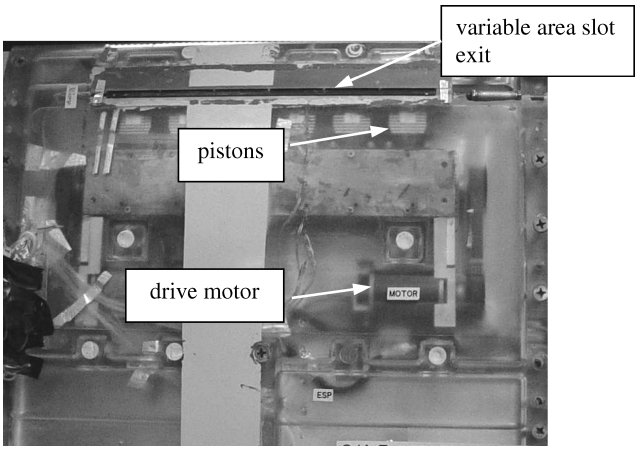

Fig. 1 Synthetic jet actuator mounted in airfoil.

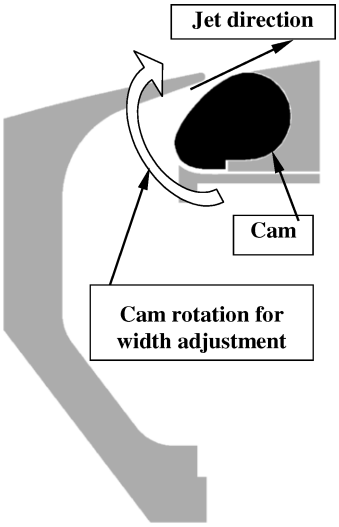

Fig. 2 SJA exit cross section showing slot design details.

Each piston has a diameter of 27.7 mm and a peak-to-peak piston stroke of 22 mm. Each dc motor measures 69.8 mm in length and 41.1 mm in diameter, has a maximum power of 800 W, and weighs 0.34 kg. The exit slot of the plenum is curved in order to permit the jet to exit tangentially to the surface of the airfoil, taking advantage of the Coanda effect. The cylinders had to be properly phased in order to reduce array vibration. This phasing in turn required the compartmentalization of the plenum, as it is obvious that if the plenum were not divided into six individual compartments, each one corresponding to each of the six cylinders, the engine phasing would result in zero net volume change in the plenum during an operation cycle and thus no synthetic jet effect. The plenum and exit slot in the actuator were designed such that the exit area was dynamically adjustable, through the use of a rotating cam connected to a stepper motor (details shown in Fig. 2). This capability is being used to develop a closed-loop pitch controller and was not used in the experiments reported in this study. The exit width could be varied from 0 to 1.3 mm. Using a feeler gauge, the slot exit width could be set to within 0.1 mm. The length of slot over each piston chamber was 41 mm. More details on the design and fabrication of the actuator can be found in Refs. 10 and 11.

The wind-tunnel model, presented in Figs. 3 and 4, was machined in two halves using a computer numerically controlled (CNC) mill. The airfoil's profile was that of a NACA 0015. The upper airfoil half was made from Plexiglas®. The lower surface was machined from aluminum. The airfoil chord was 420 mm. Tests were undertaken in Texas A&M University's 0.914 m (3 ft) by 1.22 m (4 ft) continuous wind tunnel at a freestream velocity of 20 m/s, giving a chord-based Reynolds number of 0.57×10^6. Boundary-layer transition was enforced using trip strips located at approximately 5% of the chord on the upper and lower surfaces. Surface flow visualization indicated that the trips where successful in promoting transition. No wind-tunnel wall interference or blockage corrections were applied to the data, as their application for dynamic motions is uncertain at best. Also, the current tests are comparative, and as such all data would contain similar wind-tunnel wall effects. The airfoil contained the synthetic jet actuator described earlier. All instrumentation was self-contained in the airfoil and will be described subsequently. The SJA exit slot was located at 12% of the chord. This location was chosen for two reasons: studies[19,27] have shown successful implementation of SJA control with the exit port in this location for NACA 4 series profiles, and the size of the employed SJA necessitated that it be positioned in the thickest part of the airfoil, which resulted in an exit slot at 12% chord.

The performance of the SJA actuator is documented in Figs. 5–7. Measurements were performed using a TSI model 1054 hot-wire anemometer, with the sensor located as shown. Prior to performing the measurements, the stability and damping of the anemometer were set to maximize frequency response for the highest expected SJA exit velocity. The hot wire was then calibrated; a quadratic equation was used to relate measured velocity to bridge voltage. Velocities are estimated to be accurate to within 0.5% for a 95% confidence interval. Figure 5 shows normalized time and velocity for four data sets. Time was normalized using the period of one cycle. The presented data were derectified to show the correct sign of the velocity throughout the cycle. As can be seen, the exit/inlet velocities are, generally, sinusoidal, with little effect caused by frequency or slot exit width apparent. Figure 6 investigates effects of compressibility.

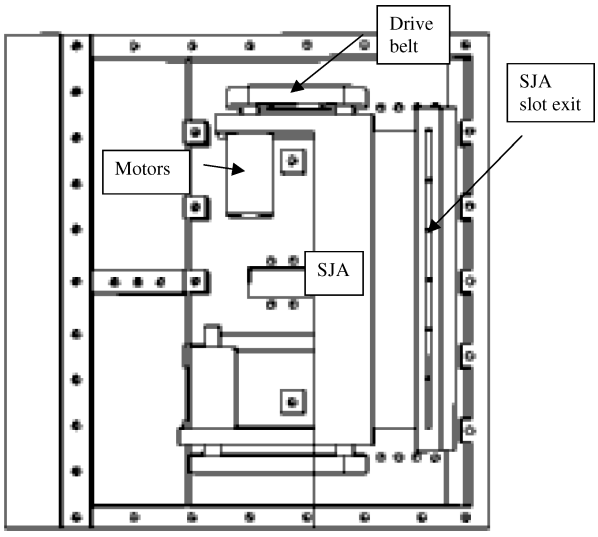

a)

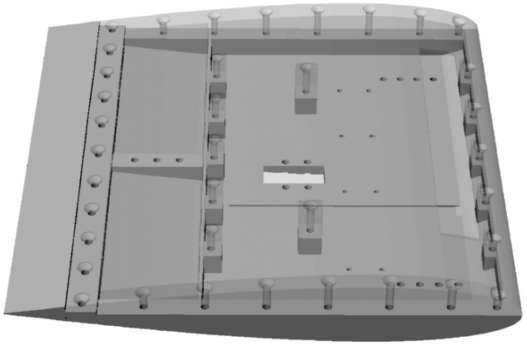

b)

Fig. 3 Wind-tunnel model details: a) internal structure and b) assembled Plexiglas (top) and aluminum (bottom) halves.

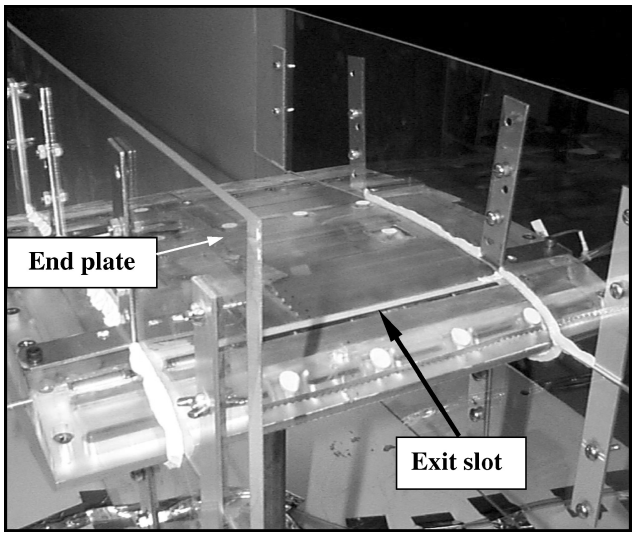

Fig. 4 Assembled airfoil installed in 3 by 4 ft wind tunnel.

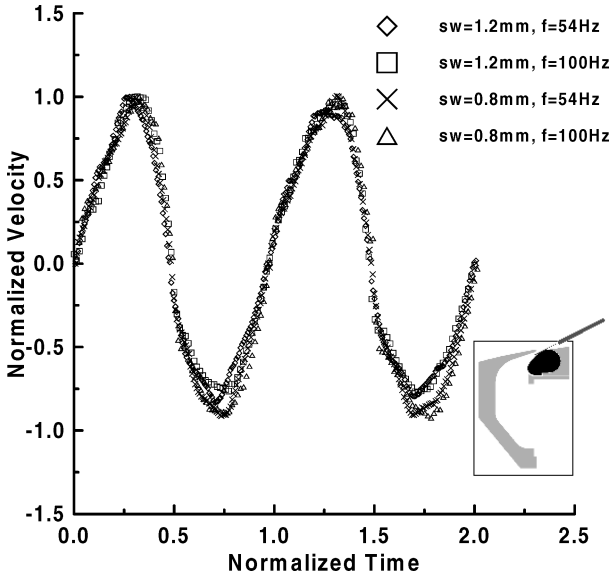

Fig. 5 Effect of SJA frequency and slot width on normalized SJA exit velocity.

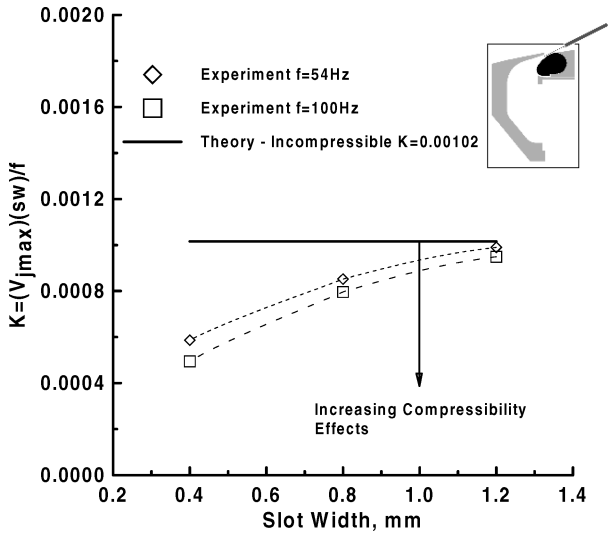

Fig. 6 Effect of compressibility on the jet exit parameter *K*.

The parameter K (determined from the continuity equation) should be a constant for a given piston and stroke combination if the flow behaves as incompressible. As can be seen, for a 1.2-mm slot the flow is incompressible. Reducing the slot width shows significant compressibility effects. An SJA frequency of 100 Hz shows greater compressibility effects than 54 Hz. SJA performance, quantified in terms of exit velocity, is presented in Figs. 7a and 7b. For a 1.2-mm slot exit, exit velocity is seen to vary essentially linearly with actuator frequency, reflecting the marginal effect of compressibility for this geometry. The maximum velocity measured at the slot exit is also indicated for slot widths of 0.4 and 0.8 mm. Although the sparse nature of the data mitigates establishment of characteristic trends, the form of the data suggests a somewhat linear dependence of velocity on frequency in this range. Maximum jet exit velocity as a function of slot exit width for two driving frequencies is detailed in Fig. 7b. As continuity considerations might infer, reducing the slot exit width increases jet exit velocity; however, compressibility effects lessen the relative increase in velocity. Nonetheless, for a 0.4-mm slot exit an exit velocity of 124 m/s (peak) was recorded ($f = 100$ Hz).

Surface pressures were measured over the airfoil using a 32-channel electronic scanning pressure (ESP) pressure scanner. The ranges of the 32 embedded transducers was ± 10 in H_2O

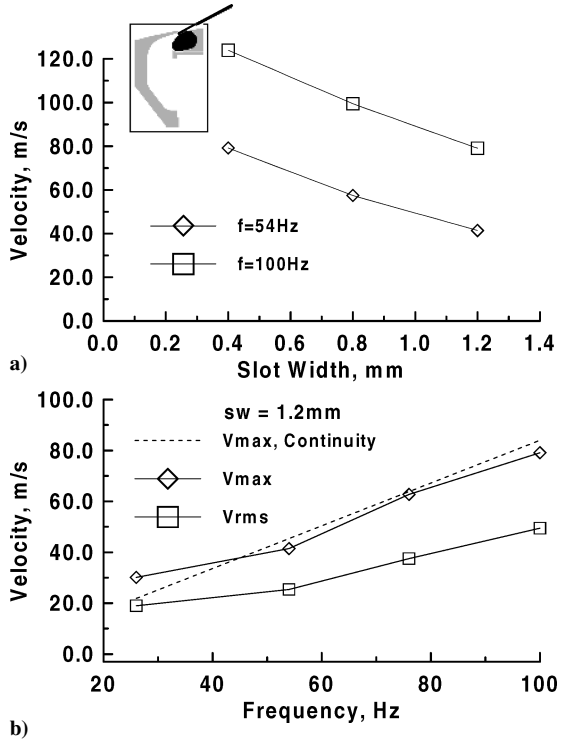

Fig. 7 Effect of frequency and slot width on SJA exit velocity: a) velocity dependence on frequency *sw* = 1.2 mm, and b) maximum SJA exit velocity as a function of slot width.

(± 2.49 kPa). Scanning rate is given by the manufacturer as 20 kHz. Location of the ports is shown in Fig. 8 and Table 1. Prior to use, the ESP was calibrated using an Edwards's barocel as a reference. Sequential checks of the validity of the calibration indicated pressure deviations of no more then 0.3% of the calibration values. To account for acoustic effects, the transfer function for the tubing connecting the surface pressure tappings to the ESP was determined using an acoustic test facility.[28] The results indicated that the tubing was over damped. Consequently, the instantaneous pressures were corrected for lag effects using the method of Wildhack[29] as this method is simple to apply, but is only applicable for over damped systems. To ensure quasi-two-dimensional behavior, side plates were mounted on the wing, as shown in Fig. 4. Subsequent data presentation will suggest that the small size of the end plates did not allow the achievement of two-dimensional flow. However, mechanical pitching considerations eliminated the use of large plates. Using separate supported side plates can cause problems because of the gap, which has to be small, which in turn can cause alignment problems in concert with a dynamic system. Forces and moments were calculated through integration of the pressure distribution around the airfoil. The upper- and lower-surface pressure traces were fitted using cubic splines. The splines were then integrated to yield forces and moments. Presented moment coefficients are about the quarter-chord.

A schematic of the experimental setup is presented in Fig. 9. The airfoil pitching motion was controlled using a stepper motor (SLO-SYN) controlled by a microlynx^{TM} stepper motor controller. The pitch axis was located at 45% of the chord. During a pitch test, airfoil position was recorded using an encoder mounted on the stepper shaft. Data from the ESP were digitized using a 16-bit computer boards A/D board. Each presented data set is comprised of 30 ensemble averages runs. Uncertainty in the measured angle of attack was estimated through repeated ramp motions in addition to static checks as well. The ramp motions indicated an uncertainty in the instantaneous angle of attack of 0.2 deg. Static checks indicated angular positioning capability within 0.1 deg. Comparison of similar data runs containing 5, 10, and 30 ensemble averages indicated that the instantaneous pressure distributions had low noise and were highly repeatable. As just mentioned, the estimated uncertainty in the indicated pressure was approximately 0.3%.

Results and Discussion

In all experiments, the airfoil was ramped at a constant angular velocity from 0 to 27 deg. Data are presented detailing the effects of the SJA on surface pressure, force, and moments. As the SJA frequency was much larger then the ramp rate, a phase relationship was unecessary.[17] Only upper surface pressures are shown, as the data indicated marginal effects on the windward surface for all tested configurations. The SJA exit slot width was 1.2 mm unless mentioned otherwise.

Table 2 presents a summary of the jet-momentum coefficients for the experimental data. All of the $C\mu$ values fall in the effective range as discussed by Lorber et al.[30] The jet-momentum coefficient indicates the momentum content of the jet; levels of lift augmentation can also indicate how effectively it is used. The rms of the jet exit velocity was calculated using the aforementioned hot-wire anemometer data. Note that decreasing the slot width to 0.4 from 0.8 mm does not increase the jet momentum because of compressibility effects lessening the exit velocity. The uncertainty in $C\mu$ is estimated at ≈2%. Also included in Table 2 is the jet's velocity ratio $V_{\max}/U$, also determined using hot-wire data.

Studies infer that global SJA effectiveness is weakly affected by F^+ in the range of $0.5 < F^+ < 1.5$[12,31] This F^+ range also approximately corresponds to that which has been generally accepted as optimal for fluidic actuation.[19] However, the effect of $C\mu$ is stronger; an insufficient $C\mu$ will not see effective flow control established,[30] whereas high $C\mu$ can establish control even at nonoptimal F^+ (Ref. 30) and can lead to saturation or insensitivity to $C\mu$. For the data presented in this study, $C\mu$ and F^+ are coupled, with most F^+ values in the optimal range. As such, the aerodynamic characteristics presented herein are evaluated in their dependency on $C\mu$, as it is inferred from prior studies that F^+ effects will be weak (for the range evaluated).

The effects of $C\mu$ on the calculated lift and pitching moment are presented in Fig. 10. Values of $C\mu$ from 0 to 0.019 are presented. The slot exit width sw was set to 1.2 mm. As noted, prior studies[22] have suggested that depending on the SJA configuration and requirement a value of $F^+ \approx 1$ is optimal as it corresponds to the presence of approximately two to four convecting vortical structures over the upper surface. The airfoil was ramped linearly at a nondimensional rate of 0.009 (corresponding to ramping the airfoil through 27 deg in 1 s). Measurements of the lift-curve slopes give values of $\approx 0.8\pi$, suggesting that the end plates were not totally successful in achieving two-dimensional flow. However, as mentioned earlier, this is not significant because of the comparative nature of this investigation. The data indicate the formation of a D.S.V. for all values of $C\mu$ presented. D.S.V. formation is also associated with a significant nose-down pitching moment because of the streamwise advection of the vortex and its associated induced localized loading. Fluidic actuation significantly delays the onset of D.S.V. formation by approximately 6-deg incidence. The data show that

Table 1 Pressure tapping locations

x/c,[a] upper	y/c,[b] upper	x/c, lower	y/c, lower
0	0	0.05	0.044
0.025	0.032	0.1	0.058
0.05	0.044	0.2	0.071
0.075	0.052	0.3	0.074
0.15	0.066	0.4	0.072
0.175	0.069	0.5	0.065
0.2	0.071	0.6	0.056
0.225	0.073	0.7	0.045
0.25	0.074	0.8	0.031
0.3	0.074	0.9	0.016
0.35	0.074	——	——
0.4	0.072	——	——
0.45	0.069	——	——
0.5	0.065	——	——
0.55	0.061	——	——
0.6	0.056	——	——
0.65	0.050	——	——
0.7	0.045	——	——
0.75	0.038	——	——
0.8	0.031	——	——
0.85	0.024	——	——
0.9	0.016	——	——

[a]x/c-axial coordinate. [b]y/c-vertical coordinate.

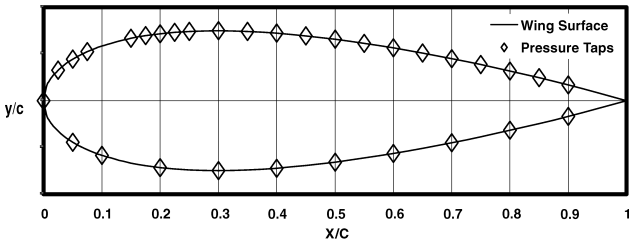

Fig. 8 Location of surface pressure tappings.

Table 2 Jet-momentum coefficient and velocity ratio summary

sw, mm	$C\mu$	F^+	$V_{\max}/U$
0.4	0.013	1	3.96
0.6	0.012	1	3.5
0.8	0.013	1	2.9
1.2	0.009	1	2.1
1.2	0.019	1.4	3.1
1.2	0.0048	0.66	1.7
1.2	0.0023	0.33	1.5

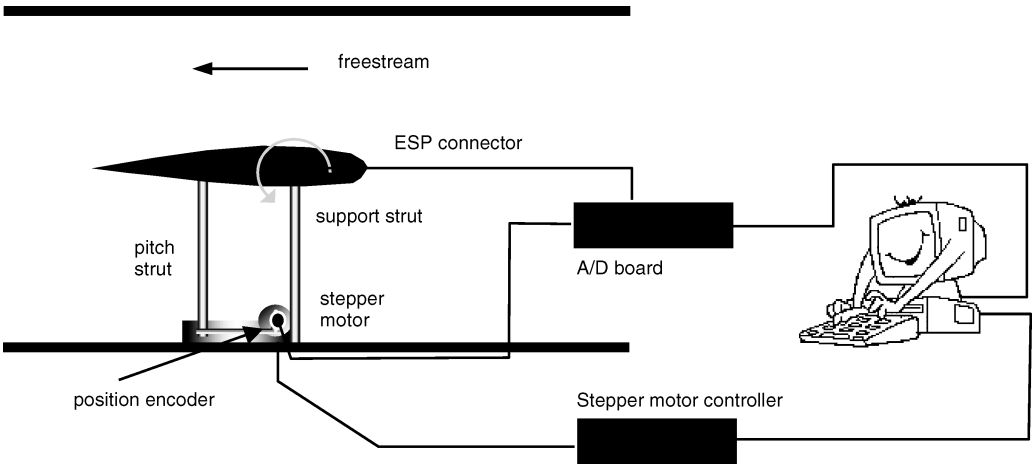

Fig. 9 Schematic of experimental setup.

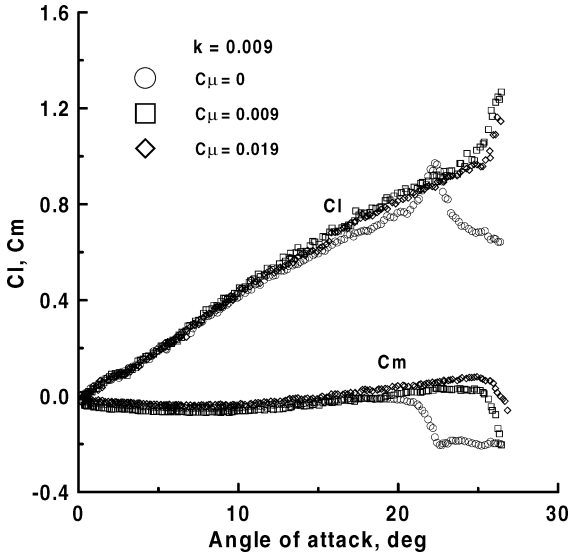

Fig. 10 Comparison of unforced ($C\mu = 0$) and forced ($C\mu \neq 0$) effects on integrated lift and pitching-moment coefficient.

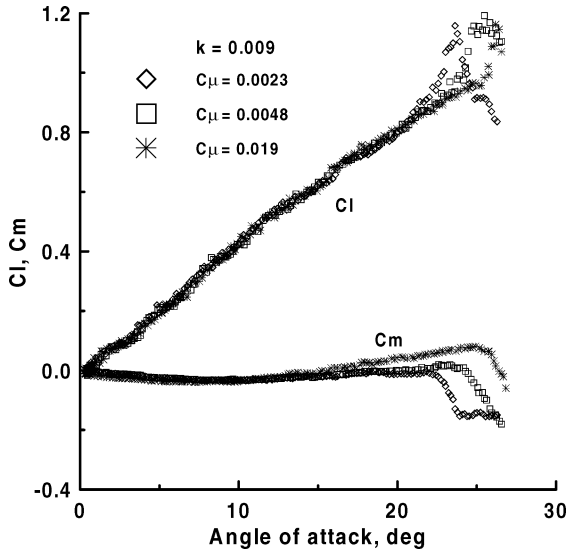

Fig. 11a Systematic effects of SJA $C\mu$ on integrated lift and pitching-moment coefficient.

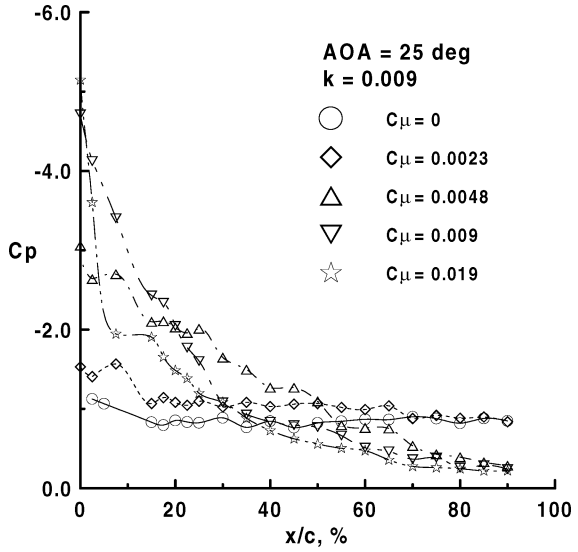

Fig. 11b Effect of SJA $C\mu$ on measured upper surface pressures.

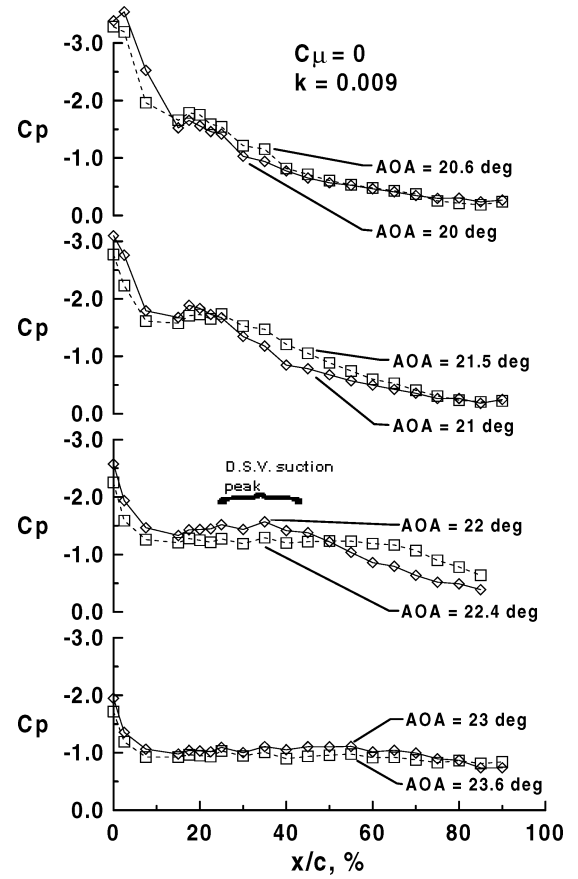

Fig. 11c Effects of airfoil incidence on upper surface-pressure trace evolution, with $C\mu = 0$.

the initial "rounding" of the *Cl*—angle-of-attack curve, indicating trailing-edge boundary layer thickening and separation, is lessened with actuation. When formed, the strength of the D.S.V. appears to be enhanced compared to the $C\mu$ or $F^+ = 0$ case. This might be because of the ability of the SJA to effectively organize the separated shear layer into a coherent structure and keep it in closer proximity to the airfoil surface. Comparing $F^+ = 0.019$ to $F^+ = 0.009$ shows only a marginal delay in D.S.V. formation (inferences are clearer from the *Cm* data), suggesting that these $C\mu$ values might be sufficient for saturation.

For greater presentational clarity, systematic variations of $C\mu$ are explored in Fig. 11a. Increasing $C\mu$ in this range is seen to delay D.S.V. formation. It can be seen that the D.S.V.-induced surface loading (i.e., difference between the peak loading and that at D.S.V. inception) is greater for $C\mu = 0.0023$ and 0.0048 than 0.019, despite this four-fold increase in $C\mu$. This might be caused by the time frame in the ramp motion where the D.S.V. forms, e.g., for $C\mu = 0.0023$, the vortex forms before the completion of the ramp motion; airfoil kinematics can thus cause closer airfoil vortex spacing then for $C\mu = 0.019$, where vortex inception occurs just before termination of the motion. An alternative explanation might be because of the nature of the jet formed by the SJA. For $C\mu = 0.0023$ and 0.0048, the jet velocity ratio is 1.5 and 1.7, which is approximately the same as the potential flow velocity adjacent to the airfoil surface (inferred, using Bernoulli's equation off surface-pressure plots 8 not included for conciseness aft of the SJA slot). Thus the jet exit velocity and the potential flow would have similar velocities. For $C\mu = 0.019$, the jet velocity ratio is approximately 3 (while the near-wall potential flow velocity is about 1.8), so the SJA forms an oscillating overdriven wall jet. Consequently, the shear layer that forms the D.S.V. after boundary layer eruption/separation would contain vorticity of both signs (as the jet velocity gradient changes sign—without separation) reducing the total circulation forming the D.S.V.

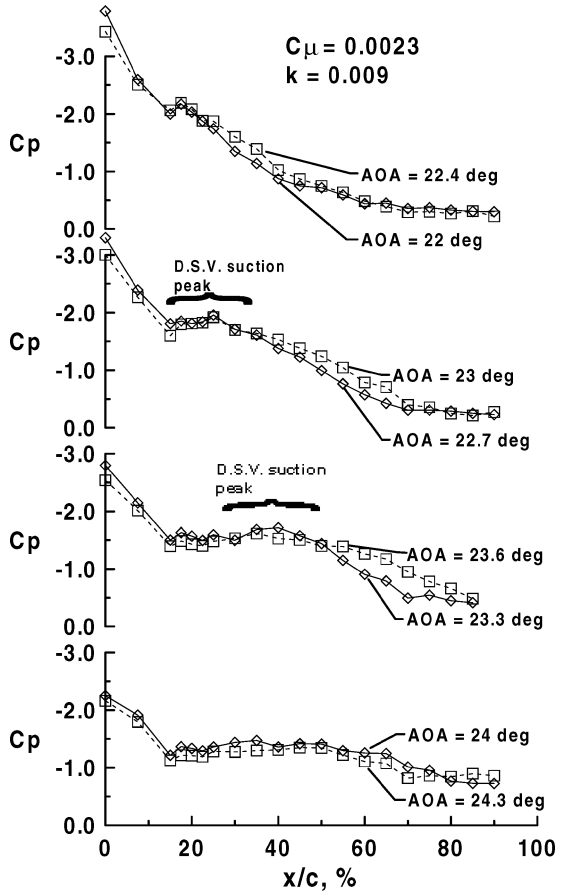

Fig. 11d Effects of airfoil incidence on upper surface-pressure trace evolution, with $C\mu = 0.0023$.

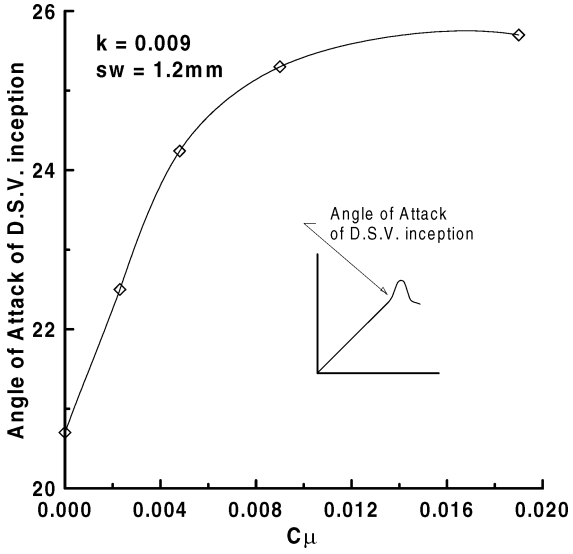

Fig. 11e Effect of $C\mu$ on D.S.V. formation incidence.

Figure 11b shows a "snapshot" of the instantaneous upper surface-pressure distribution when the airfoil incidence equaled 25 deg. Clearly, the no actuation case, $F^+ = 0$, shows massive upper-surface flow separation with an essentially flat pressure distribution. A similar distribution is seen for $C\mu = 0.0023$, where the D.S.V. has already advected off the airfoil as can be inferred from the loading presented in Fig. 11a. Higher values of $C\mu$ show the presence of a leading-edge suction peak, with $C\mu = 0.019$ showing the highest overall leading-edge suction levels. Figure 11c shows the systematic evolution of the upper surface-pressure distribution as a function of incidence for $C\mu = 0$. Although somewhat weak, the effect of the

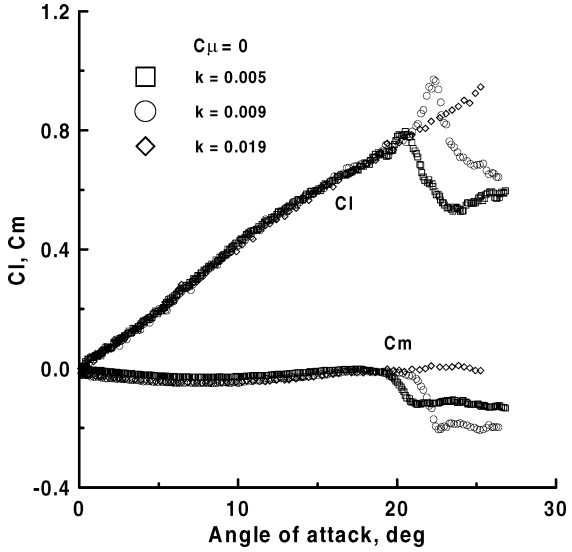

Fig. 12a Effects of airfoil ramp rate k on integrated lift and pitching-moment coefficient, with $C\mu = 0$.

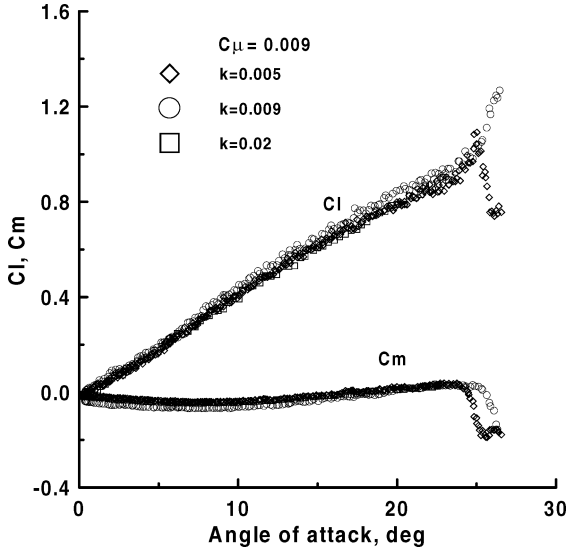

Fig. 12b Effects of airfoil ramp rate k on integrated lift and pitching-moment coefficient, with $C\mu = 0.009$.

D.S.V. is seen as a localized "hump" in the pressure distribution that advects downstream. The presence of the D.S.V. is also indicated by a significant reduction if not elimination of the leading-edge suction peak. Figure 11d presents similar data with SJA actuation, $C\mu = 0.0023$. Similar characteristics to those detailed in Fig. 11c are seen, except the D.S.V. peak is somewhat larger. The effect of $C\mu$ on the D.S.V. formation incidence is presented in Fig. 11e. These angles were determined from examination of the lift and pitching-moment data. As such, they do not necessarily represent the exact angle at which the vortex started formation, but rather that at which its effect on Cl and Cm became noticeable. The plot suggests that within the limitations of the sparse data set the delay in D.S.V. inception with increasing $C\mu$ is roughly linear for $C\mu < 0.006$.

The effect of the nondimensional ramp rate k is explored in Figs. 12a and 12b, with and without actuation. Ramp rates of $k = 0.005$ (27 deg in 2 s), 0.009 (27 deg in 1 s), and 0.019 (27 deg in 0.5 s) are presented. The data in Fig. 12a ($C\mu = 0$) display the expected effects of ramp rate. As k increases, the linear portion of the lift curve is extended. For the lowest ramp rate $k = 0.005$, the data do not show clear evidence of a D.S.V. formation. Increasing k to 0.009 shows the formation of a D.S.V. at approximately 21-deg incidence. A marked nose-down moment is indicated at the D.S.V. onset. The highest ramp rate $k = 0.019$ shows an extension

of the linear portion of the lift-curve to 27 deg (corresponding to the highest achievable incidence, equipment limitations precluding higher incidences). Notice the form of the pitching-moment break for $k = 0.005$ and 0.009. The plot for the higher ramp rate shows a small moment reversal corresponding to the incidence at which the lift data suggest that the D.S.V. has passed off the airfoil, approximately 22.5 deg.

Figure 12b shows the effects of SJA actuation for the same ramp motions as presented in Fig. 12a. The data show that actuation causes D.S.V. formation for $k = 0.005$, which was not present without actuation (see Fig. 12a). This is most likely caused by the SJA forcing causing the separating shear layer to roll up into a coherent vortical structure or D.S.V. Without actuation, for this ramp rate the flow separates, and the airfoil stalls in a psuedosteady manner. As seen and documented prior for higher ramp rates, the SJA has the effect of delaying D.S.V. formation to higher incidence.

Figure 13a shows the effect of two slot widths on calculated Cl and Cm for $F^+ = 1$ and $k = 0.009$. Notice that for the data presented the sw does not have an effect on the airfoil incidence angle at which the D.S.V. forms (as can be inferred off the Cm plot, despite a 33% difference in $C\mu$, suggesting saturation). Figure 13b shows a snapshot of the upper surface pressures at a airfoil incidence of 25 deg for fixed slot widths of 0.4, 0.8, and 1.2 mm. The largest slot width 1.2 mm ($C\mu = 0.009$) shows the largest suction peak but diminished loading over the midchord of the airfoil compared to slot widths of 0.4 mm ($C\mu = 0.013$) and 0.8 mm ($C\mu = 0.013$). The bigger slot, caused by lessened compressibility effects, would have greater inflow into the plenum then the smaller slot, causing an increase in loading upstream of the slot. Dowstream of the slot, the smaller slots higher exit velocity (see Table 2) may yield greater loading in this region.

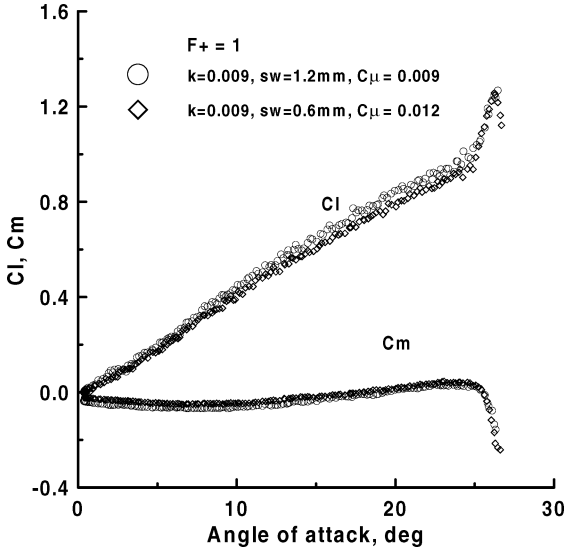

Fig. 13a Effects of slot width sw on integrated lift and pitching-moment coefficient, with $F^+ = 1$.

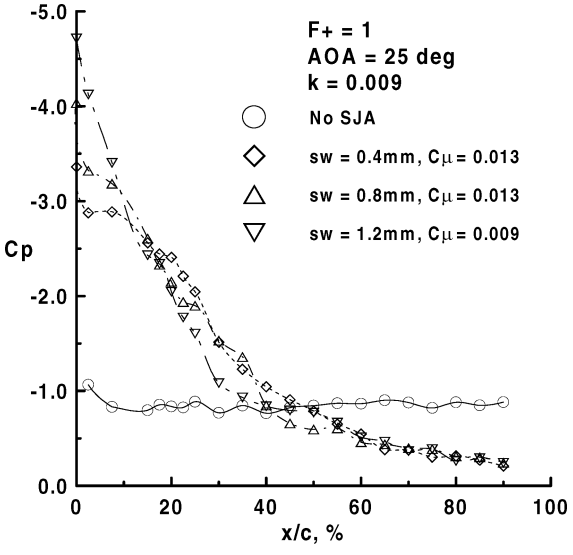

Fig. 13b Effect of slot width sw on measured upper surface pressures.

To gain an insight into the flow physics associated with the fluidic actuation, a hot-wire anemometer survey was conducted over the airfoil. The flow adjacent to the upper airfoil surface was traversed, with the probe displacement perpendicular to the surface. A cosine point spacing was used, with the traverse containing 25 points in the Z_{normal} direction. At each point, approximately 8000 readings were collected at 8 kHz. Temporal phasing was achieved using an encoder signal connected to the motor shaft. The quantity of data collected facilitated phase averaging; each set represents 25 averages (data comparisons for 25 and 50 averages showed close accord). The survey was conducted with the probe located axially at 32% of the chord (when at the closest position to the airfoil surface) and the airfoil at a fixed 20-deg incidence. Data from these surveys are summarized in Fig. 14. Plots are presented showing the instantaneous phase-averaged velocity profiles at successive time instants throughout one cycle of the SJA. The data clearly shows the direct boundary layer injection of momentum caused by actuation. During the midcycle $t = 0.5T$, the boundary layer profile is seen to be significantly "filled" out, whereas at the beginning and towards the end of the stroke cycle ($t = 0T$ and $0.875T$) there is a velocity deficit towards the surface associated with a conventional boundary layer profile. Further away from the airfoil surface $Z_{\text{normal}}/c > 0.03$, the velocity is seen to be approximately uniform and similar for all time instants.

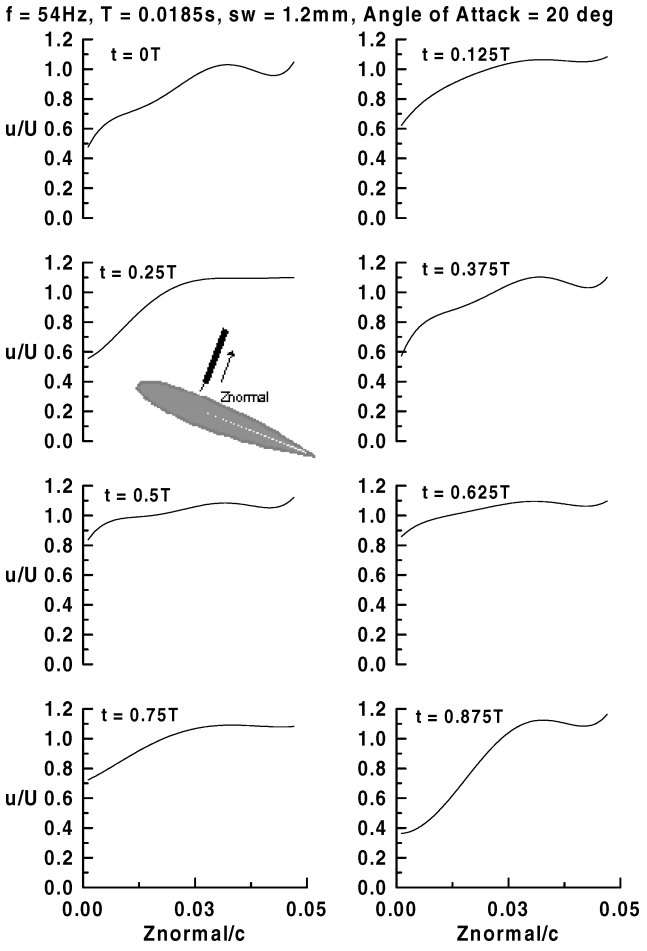

Fig. 14 Instantaneous temporally phase-averaged velocities measured aft of the SJA, with $F^+ = 1$ and $C\mu = 0.009$.

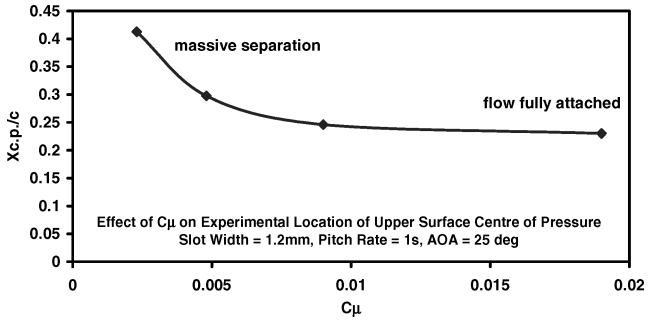

Fig. 15 Effect of $C\mu$ on location of upper-surface center of pressure.

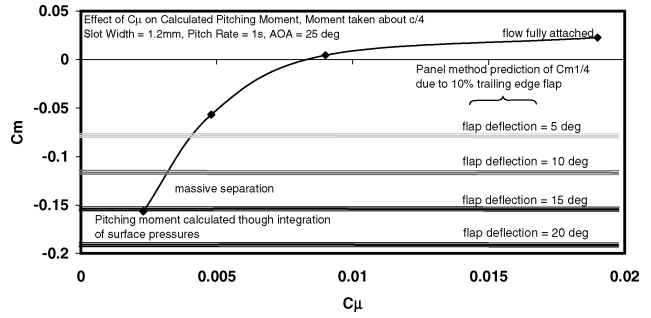

Fig. 16 Effect of $C\mu$ on calculated quarter-chord pitching moment.

The hot-wire data shown in Fig. 7 indicates that for the SJA operating conditions presented in Fig. 14 $V_{\text{rms}} \approx 25$ m/s ($V_{\text{rms}}/U = 1.25$) and $V_{\max} \approx 41$ m/s ($V_{\text{rms}}/U = 2.05$). These jet exit velocities were measured in the absence of a freestream, but it would be expected that the impact of a freestream, and thus reduced exit pressures, would be to increase the exit velocities during the ejection cycle and decrease them during the inflow cycle. The data in Fig. 14 show no apparent "jetting" in the near surface boundary layer, although the jet velocity ratios just mentioned suggest that the exit velocities are of sufficient magnitude for temporal jetting to be present. The hot-wire measurement plane was 20% (84 mm) behind the SJA exit and indicates the rapid attenuation of the jet caused by viscosity and spreading.

The preceding results indicate that in the tested flow regime upper surface pressures can be independently manipulated though SJA drive frequency and to a lesser extent slot width variations. This is explored more thoroughly in Figs. 15 and 16, which present the location of the section's center of pressure and quarter-chord pitching moment as a function of $C\mu$ respectively. For these figures the slot width was 1.2 mm with $k = 0.009$. Variation of the actuator $C\mu$ (from 0.0023 to 0.019) is seen to cause significant movement of the center of pressure (as increasing $C\mu$ results in more complete flow reattachment such that the c.p. location approaches the theoretical potential flow location, i.e., $X_{\text{c.p.}}/c = 0.25$). Locations indicating massively separated flow ($C\mu = 0.0023$, $X_{\text{c.p.}}/c = 0.42$) to fully attached ($C\mu = 0.019$, $X_{\text{c.p.}}/c = 0.25$) are indicated. The effects of these large changes in the center of pressure are quantified in Fig. 15. For reference, the figure also displays predicted pitching moments that deflection of a 10% trailing-edge flap would generate. These estimates were calculated using a Smith–Hess panel method. The data clearly show that nose-down pitching moments, comparable in magnitude to those achievable through a conventional trailing-edge control device, can be generated through control of the extent of flow separation. Naturally, this form of fluidic control would only be of value at high angles of attack; alternative flow control methods would have to be found to achieve hingeless control in attached flow regimes.

Summary

A low-speed wind-tunnel investigation has been undertaken to determine the effect of synthetic jet actuation on an airfoil performing a linear ramping motion. An instrumented NACA 0015 airfoil was ramped from 0 to 27 deg at various ramp rates during which surface pressures were recorded. The actuators frequency and slot exit width were varied. Presented data included surface pressures as well as integrated parameters. The instantaneous behavior of the synthetic jet was characterized using a hot-wire anemometer. The data indicated that small slot exit widths were prone to compressibility effects (reduced exit velocities), with driving frequency having a smaller, yet similar deleterious effect.

The data show that fluidic oscillation delays the onset of the dynamic-stall vortex formation to higher airfoil incidence angles. When formed, the stall vortex appears to induce higher loading then in the unforced case. For low ramp rates with no synthetic jet actuation, a stall vortex was not observed. For the same motion, forcing caused stall vortex formation, presumably due to the ability of the forcing to control and structure the separating shear layer. Instantaneous velocities measured above the airfoil surface showed that for the SJA tested the effect of the actuator was to directly inject momentum into the boundary layer.

Acknowledgments

This work was sponsored by the U.S. Air Force Office of Scientific Research (AFOSR), under the Contract Number F49620-01-1-0012 and by U.S. Air Force Research Laboratory through the U.S. Department of Defense small business initiation research (SBIR) Program (in collaboration with Aeroprobe Corporation). The authors would like to thank Thomas Beutner, the technical monitor for the AFOSR project, and James Myatt and Chris Camphouse, the technical monitors of the SBIR project. The authors would also like to thank Rick Allen and John Januskey for their help with the experimental component fabrication.

References

[1]Klausmeyer, S. M., Papadakis, M., and Lin, J. C., "A Flow Physics Study of Vortex Generators on a Multi-Element Airfoil," AIAA Paper 96-0548, Jan. 1996.

[2]Chang, R. C., Hsiao, F. B., and Shyu, R. N., "Forcing Level Effects of Internal Acoustic Excitation on the Improvement of Airfoil Performance," *Journal of Aircraft*, Vol. 29, No. 5, 1992, pp. 823–829.

[3]Huang, R. F., and Mao, S. W., "Separation Control on a Cantilever Wing with a Self-Excited Vibrating Rod," *Journal of Aircraft*, Vol. 39, No. 4, 2002, pp. 609–615.

[4]Tillman, T. G. and Hwang, D. P., "Drag Reduction on a Large-Scale Nacelle Using a Micro-Blowing Technique," AIAA Paper 99-0130, Jan. 1999.

[5]Kruger, W., "Drag Reduction by Suction of the Boundary Layer Separated Behind Shock Wave Formation at High Mach Numbers," NACA TM 1168, July 1947.

[6]Modi, V. J., Munshi, S. R., Bandyopadhyay, G., and Yokomizo, T., "High-Performance Airfoil with Moving Surface Boundary-Layer Control," *Journal of Aircraft*, Vol. 35, No. 4, 1998, pp. 544–553.

[7]Sun, M., and Hamdani, H., "Separation Control by Alternating Tangential Blowing/Suction at Multiple Slots," AIAA Paper 01-0297, Jan. 2001.

[8]Choi, K.-S., and Clayton, B. R., "The Mechanism of Turbulent Drag Reduction with Wall Oscillation," *International Journal of Heat and Fluid Flow*, Vol. 22, Feb. 2001, pp. 1–9.

[9]Ashpis, D. E., and Reshotko, E., "The Vibrating Ribbon Problem—Revisited," *Journal of Fluid Mechanics*, Vol. 213, April 1990, pp. 531–547.

[10]Gilarranz, J. L., Traub, L. W., and Rediniotis, O. K., "Characterization of a Compact, High-Power Synthetic Jet Actuator for Flow Separation Control," AIAA Paper 2002-0127, Jan. 2002.

[11]Gilarranz, J. L., and Rediniotis, O. K., "Compact, High-Power Synthetic Jet Actuators for Flow Separation Control," AIAA Paper 2001-0737, Jan. 2001.

[12]Amitay, M., and Glezer, A., "Role of Actuation Frequency in Controlled Flow Reattachment over a Stalled Airfoil," *AIAA Journal*, Vol. 40, No. 2, 2002, pp. 209–216.

[13]Amitay, M., Smith, D. R., Kibens, V., Parekh., D. E., and Glezer, A., "Aerodynamic Flow Control over an Unconventional Airfoil using Synthetic Jet Actuators," *AIAA Journal*, Vol. 39, No. 3, 2002, pp. 361–370.

[14]Tuncer, I. H., and Platzer, M. F., "Computational Study of Flapping Airfoil Aerodynamics," *Journal of Aircraft*, Vol. 37, No. 3, 2000, pp. 514–520.

[15]Tuncer, I. H., Lai, J., Ortiz, M. A., and Platzer, M. F., "Unsteady Aerodynamics of Stationary/Flapping Airfoil Combination in Tandem," AIAA Paper 97-0659, Jan. 1997.

[16]Wu, J. Z., Lu, X., Denny, A. G., Fan, M., and Wu, J., "Post-Stall Flow Control on an Airfoil by Local Unsteady Forcing," *Journal of Fluid Mechanics*, Vol. 371, 1998, pp. 21–58.
[17]Greenblatt, D., and Wygnanski, I., "Dynamic Stall Control by Periodic Excitation, Part 1: NACA 0015 Parametric Study," *Journal of Aircraft*, Vol. 38, No. 3, 2001, pp. 430–438.
[18]Greenblatt, D., Darabi, A., Nishri, B., and Wygnanski, I., "Separation Control by Periodic Addition of Momentum with Particular Emphasis on Dynamic Stall," *Proceedings of Heli Japan 98*, American Helicopter Society, Paper T3-4, April 1998.
[19]Seifert, A., and Pack, L., "Oscillatory Control of Separation at High Reynolds Numbers," *AIAA Journal*, Vol. 37, No. 9, 1999, pp. 1062–1071.
[20]Seifert, A., and Pack, L., "Oscillatory Excitation of Unsteady Compressible Flows over Airfoils at Flight Reynolds Number," AIAA Paper 99-0925, Jan. 1999.
[21]Amitay, M., Smith, B. L., and Glezer, A., "Aerodynamic Flow Control Using Synthetic Jet Technology," AIAA Paper 98-0208, Jan. 1998.
[22]Seifert, A., Eliahu, S., Greenblatt, D., and Wygnanski, I., "On the Use of Piezoelectric Actuators for Airfoil Separation Control," *AIAA Journal*, Vol. 36, No. 8, 1998, pp. 1535–1537.
[23]Smith, D., Amitay, M., Kibens, V., Parekh, D., and Glezer, A., "Modifications of Lifting Body Aerodynamics Using Synthetic Jet Actuators," AIAA Paper 98-0209, Jan. 1998.
[24]Ericsson, L. E., "Dynamic Stall of Pitching Airfoils and Slender Wings—Similarities and Differences," AIAA Paper 98-0414, Jan. 1998.
[25]Shih, C., and Ding, Z., "Vortex Interaction of a Delta-Wing Flowfield," *AIAA Journal*, Vol. 41, No. 2, 2003, pp. 314–316.
[26]Ferrecchia, A., Coton, F. N., and Gailbraith, R. A., "An Examination of Dynamic Stall Vortex Inception on a Finite Wing and on a NACA 0015 Aerofoil," AIAA Paper 1999-3112, June–July 1999.
[27]Hassan, A. A., and JanakiRam, R. D., "Effects of Zero-Mass 'Synthetic' Jets on the Aerodynamics of the NACA 0012 Airfoil," *Journal of the American Helicopter Society*, Vol. 47, No. 4, 1998.
[28]Johansen, E. S., "Development of a Fast-Response Multi-Hole Probe for Unsteady and Turbulent Flowfields," Ph.D. Dissertation, Aerospace Engineering Dept., Texas A&M Univ., College Station, Dec. 2001.
[29]Wildhack, W. A., "Pressure Drop in Tubing in Aircraft Instrument Installations," NACA TN-593, Feb. 1937, p. 30.
[30]Lorber, P., McCormick, D., Anderson, T., Wake, and MacMartin, B., "Rotorcraft Retreating Blade Stall Control," AIAA Paper 2000-2475, June 2000.
[31]Sun, M., and Hamdani, H., "Separation Control by Alternating Tangential Blowing/Suction at Multiple Slots," AIAA Paper 2001-0297, Jan. 2001.